



HAL
open science

Thermal shock fracture in cross-ply fibre-reinforced ceramic-matrix composites

Christos Kastritseas, Paul Smith, Julie Yeomans

► **To cite this version:**

Christos Kastritseas, Paul Smith, Julie Yeomans. Thermal shock fracture in cross-ply fibre-reinforced ceramic-matrix composites. *Philosophical Magazine*, 2010, 90 (31), pp.4209. 10.1080/14786431003785621 . hal-00606279

HAL Id: hal-00606279

<https://hal.science/hal-00606279>

Submitted on 6 Jul 2011

HAL is a multi-disciplinary open access archive for the deposit and dissemination of scientific research documents, whether they are published or not. The documents may come from teaching and research institutions in France or abroad, or from public or private research centers.

L'archive ouverte pluridisciplinaire **HAL**, est destinée au dépôt et à la diffusion de documents scientifiques de niveau recherche, publiés ou non, émanant des établissements d'enseignement et de recherche français ou étrangers, des laboratoires publics ou privés.



Thermal shock fracture in cross-ply fibre-reinforced ceramic-matrix composites

Journal:	<i>Philosophical Magazine & Philosophical Magazine Letters</i>
Manuscript ID:	TPHM-09-Aug-0342.R1
Journal Selection:	Philosophical Magazine
Date Submitted by the Author:	22-Feb-2010
Complete List of Authors:	Kastritseas, Christos; University of Surrey, Faculty of Engineering and Physical Sciences Smith, Paul; University of Surrey, Faculty of Engineering and Physical Sciences Yeomans, Julie; University of Surrey, Faculty of Engineering and Physical Sciences
Keywords:	ceramic matrix composites, cracking
Keywords (user supplied):	thermal shock



Thermal shock fracture in cross-ply fibre-reinforced ceramic-matrix composites

C. Kastritseas^{*}, P.A. Smith and J.A. Yeomans

*Faculty of Engineering & Physical Sciences, University of Surrey, Guildford, Surrey
GU2 7XH, UK*

The onset of matrix cracking due to thermal shock in a range of simple and multi-layer cross-ply laminates comprising a calcium aluminosilicate (CAS) matrix reinforced with Nicalon® fibres is investigated analytically in this study. A comprehensive stress analysis under conditions of thermal shock, ignoring transient effects, is performed and fracture criteria based on either a recently-derived model for the thermal shock resistance of unidirectional Nicalon®/glass ceramic-matrix composites or fracture mechanics considerations are formulated. The effect of material thickness on the apparent thermal shock resistance is also modelled. Comparison with experimental results reveals that the accuracy of the predictions is satisfactory and the reasons for some discrepancies are discussed. In addition, a theoretical argument based on thermal shock theory is formulated to explain the observed cracking patterns.

Keywords: ceramic matrix composites; cracking; thermal shock

1. Introduction

Fibre-reinforced ceramic-matrix composites (CMCs) exhibit better behaviour under conditions of thermal shock, i.e. when subjected to an abrupt temperature change (ΔT), than their monolithic and particulate- or whisker-reinforced counterparts [1,2]. However, although failure is avoided and damage can be accommodated, there is significant damage accumulation in the form of matrix cracks of various orientations that can lead to property degradation and may affect long-term material behaviour, especially under the presence of oxidative conditions [3-6].

Recently, a **semi-empirical** methodology has been proposed [7] that allows satisfactory predictions to be made for the onset (i.e. the critical quenching temperature differential, ΔT_c) of multiple matrix cracking due to thermal shock when heated samples of a range of dense glass ceramic-matrix CMCs containing unidirectional (UD) Nicalon® fibres are quenched into room-temperature water. The methodology, in contrast to previous work [4,8], considered the anisotropic stress field generated during the shock and the effect of thermal shock-induced stresses (as well as of residual thermal stresses) on the effective value of the interfacial shear stress that characterises the fibre-matrix interface. Utilising as inputs the processing temperature of the CMC, the temperature of the quenching medium, and room-temperature material properties, satisfactory correlation with experimental data was obtained and the heat transfer condition during the critical shock (as quantified by the 'stress reduction factor', A) was characterised.

In this paper, this methodology is complemented with new results to cover the case of cross-ply CMCs subjected to thermal shock treatment. Detailed experimental

^{*} Corresponding author. E-mail: c_kastritseas@hotmail.com

investigations using Nicalon®/calcium aluminosilicate (CAS) CMCs of various lay-ups (simple $[0/90]_s$ and $[90/0]_s$, multi-layer $[0/90]_{3s}$, $[90/0]_{3s}$ and $[0_2/90_4]_s$) [9,10] have shown that the 0° plies of water-quenched samples exhibit multiple matrix cracking perpendicular to the fibre axis (termed perpendicular matrix cracks – PMCs), similar to that observed in thermally shocked UD Nicalon®/CAS [4] and in the 0° plies of the same lay-ups under tensile loading [11]. The 90° plies of these laminates, in contrast to the multiple matrix cracking pattern they exhibit under tensile loading [11], contained one or two cracks that advanced along the ply length (termed horizontal matrix cracks – HMCs). Both damage morphologies can be seen in the image of figure 1 on a $[90/0]_{3s}$ cross-ply Nicalon®/CAS laminate.

Figure 1

Damage was always first detected at ΔT_c in the central plies of each CMC, i.e. the central 90° plies of the $[0/90]_s$, $[0/90]_{3s}$ and $[0_2/90_4]_s$ laminates and the central 0° plies of the $[90/0]_s$ and $[90/0]_{3s}$ CMCs, with the laminates with 0° central plies exhibiting slightly higher resistance to thermal shock. On application of more severe shocks, damage extended to the outer plies and displayed the same modes, i.e. PMCs in 0° plies and HMCs in 90° plies. However, crack density always displayed a gradient being maximum at the central plies and gradually decreasing towards the top and bottom corners. In addition, the thinner, simple laminates ($[0/90]_s$, $[90/0]_s$) exhibited higher thermal shock resistance than their thicker, multi-layer counterparts.

The structure of the paper is as follows: after performing a detailed stress analysis of the cross-ply laminates under thermal shock (ignoring transient effects), we formulate fracture criteria for both the 0° and the 90° plies. The effect of component thickness on thermal shock behaviour is also modelled. Subsequently, we present predictions for the thermal shock resistance of the range of cross-ply Nicalon®/CAS laminates investigated in [9] and [10]. A theoretical argument is then provided to explain why damage at fracture onset (ΔT_c) always appears at the central plies of the CMCs and why a crack density gradient exists at higher shocks.

2. The applied stress field

The stress field in a cross-ply CMC held at an initial temperature T_s comprises residual thermal stresses at the laminate level due to differential expansion of 0° and 90° plies, and residual stresses at the ply level inside the 0° plies due to differences in coefficient of thermal expansion (CTE) between fibre and matrix. To estimate the magnitudes of these stresses, we consider one of the parallel faces of a rectangular plate of cross-ply CMC with thickness t , modelled in figure 2 as a two-part system of 0° plies with total thickness t_L and 90° plies with total thickness t_T . Each 0° ply comprises a matrix of volume fraction V_m with stiffness E_m , CTE α_m and Poisson's ratio ν_m , which contains fibres of volume fraction $V_f (=1-V_m)$ with properties E_f , α_f , ν_f . The ply has properties E_1 , E_2 , ν_{12} , ν_{21} , α_1 and α_2 along its principal axes.

Figure 2

To calculate laminate-level residual stresses in the 0° (σ_L^{RES}) and 90° (σ_T^{RES}) plies, we assume that thermal strains generated after the material has been cooled from its processing temperature (T_p) remain compatible while any stresses in the y-direction are neglected. A simple force balance along the x-direction ($\sigma_L^{RES} t_L + \sigma_T^{RES} t_T = 0$) gives:

$$\sigma_L^{RES} = -\frac{t_T E_2 E_1 (\alpha_2 - \alpha_1)}{t_T E_2 + t_L E_1} \Delta T_F = \Theta_L \Delta T_F \quad (1)$$

$$\sigma_T^{RES} = \frac{t_L E_2 E_1 (\alpha_2 - \alpha_1)}{t_T E_2 + t_L E_1} \Delta T_F = \Theta_T \Delta T_F \quad (2)$$

with $\Delta T_F = T_p - T_s$. The axial residual stress at the laminate level in the matrix of the 0° ply is found by multiplying (1) with the fraction E_m/E_1 . The axial and transverse residual stresses in the matrix inside the 0° ply due to differences in CTE between fibre and matrix, $\sigma_{1,M}^{RES}$ and $\sigma_{2,M}^{RES}$, are given by [7]:

$$\sigma_{1,M}^{RES} = \frac{[1 + (E_1/E_f)] E_m E_f V_f (\alpha_m - \alpha_f)}{2[1 - [(1 - 2\nu_{12})/2(1 - \nu_{12})]] [1 - (E_1/E_f)] E_1 (1 - \nu_{12})} \Delta T_F = \Theta_1 \Delta T_F \quad (3)$$

$$\sigma_{2,M}^{RES} = -\frac{E_m (1 - V_f) (\alpha_m - \alpha_f)}{2[[1 - (1 - 2\nu_{12})/2(1 - \nu_{12})]] [1 - (E_1/E_f)] (1 - \nu_{12})} \Delta T_F = \Theta_2 \Delta T_F \quad (4)$$

When subjected to a thermal shock, the face of the material shown in figure 2 comes into contact with a cooling medium of temperature T_o . The stresses induced as a result of the thermal shock ($\Delta T = T_s - T_o$), can be found if we assume that when the surface of the material in question is instantaneously cooled from T_s to T_o (i.e. perfect heat transfer between the material and the cooling medium is assumed), it immediately adopts the temperature T_o while the other parts of the material remain at T_s . This case corresponds to having a surface that can freely expand in the z-direction (i.e. perpendicular to the plane of figure 2), with suppressed expansion in the x- and y-directions. In the absence of displacement restrictions, the 0° and 90° plies would expand along the x-direction and the y-direction by thermal strains of:

$$\varepsilon_{x,L}^{th} = \alpha_1 (T_o - T_s) \quad (5)$$

$$\varepsilon_{x,T}^{th} = \alpha_2 (T_o - T_s) \quad (6)$$

$$\varepsilon_y^{th} = (t_L/t) \alpha_2 (T_o - T_s) + (t_T/t) \alpha_2 (T_o - T_s) \quad (7)$$

Since thermal expansion in both directions is completely suppressed, elastic strains $\varepsilon_{x,L}^{el}$, $\varepsilon_{x,T}^{el}$, ε_y^{el} are created that compensate the thermal strains, therefore equations (5)-(7) give:

$$\varepsilon_{x,L}^{el} = -\varepsilon_{x,L}^{th} = -\alpha_1(T_o - T_s) = \alpha_1(T_s - T_o) = \alpha_1\Delta T \quad (8)$$

$$\varepsilon_{x,T}^{el} = -\varepsilon_{x,T}^{th} = -\alpha_2(T_o - T_s) = \alpha_2(T_s - T_o) = \alpha_2\Delta T \quad (9)$$

$$\varepsilon_y^{el} = -\varepsilon_y^{th} = -(t_L/t)\alpha_2(T_o - T_s) - (t_T/t)\alpha_2(T_o - T_s) = (t_L/t)\alpha_2\Delta T + (t_T/t)\alpha_2\Delta T \quad (10)$$

The elastic strains cause 'thermal stresses' along the principal axes of the material and can be written as:

$$\varepsilon_{x,L}^{el} = \sigma_{x,L}^{TS}/E_1 - \nu_{TL}\sigma_y^{TS}/E_2 \quad (11)$$

$$\varepsilon_{x,T}^{el} = \sigma_{x,T}^{TS}/E_2 - \nu_{TT}\sigma_y^{TS}/E_2 \quad (12)$$

$$\varepsilon_y^{el} = (\sigma_y^{TS}/E_2 - \nu_{LT}\sigma_{x,L}^{TS}/E_1)(t_L/t) + (\sigma_y^{TS}/E_2 - \nu_{TT}\sigma_{x,T}^{TS}/E_2)(t_T/t) \quad (13)$$

It can be assumed that $\nu_{LT}=\nu_{12}$, $\nu_{TL}=\nu_{21}$ and $\nu_{TT}=\nu_m$. By substituting (11)-(13) in (8)-(10), the resulting expressions for the axial thermal shock-induced stresses in the 0° and 90° plies, $\sigma_{x,L}^{TS}$ and $\sigma_{x,T}^{TS}$, as well as for the thermal shock stress component along the y-direction, σ_y^{TS} , are given by:

$$\sigma_{x,L}^{TS} = A \left\{ E_1 \alpha_1 + \frac{\nu_{TL} E_1 [t_L (\alpha_2 + \nu_{LT} \alpha_1) + t_T \alpha_2 (1 + \nu_{TT})]}{t_L (1 - \nu_{TL} \nu_{LT}) + t_T (1 - \nu_{TT}^2)} \right\} \Delta T = A Q_{x,L} \Delta T \quad (14)$$

$$\sigma_{x,T}^{TS} = A \left\{ E_2 \alpha_2 + \frac{\nu_{TT} E_2 [t_L (\alpha_2 + \nu_{LT} \alpha_1) + t_T \alpha_2 (1 + \nu_{TT})]}{t_L (1 - \nu_{LT} \nu_{LT}) + t_T (1 - \nu_{TT}^2)} \right\} \Delta T = A Q_{x,T} \Delta T \quad (15)$$

$$\sigma_y^{TS} = A \left\{ \frac{E_2 [t_L (\alpha_2 + \nu_{LT} \alpha_1) + t_T \alpha_2 (1 + \nu_{TT})]}{t_L (1 - \nu_{TL} \nu_{LT}) + t_T (1 - \nu_{TT}^2)} \right\} \Delta T = A Q_y \Delta T \quad (16)$$

As in reality perfect heat transfer conditions are not achievable, the stress reduction factor, A, which accounts for the finite value of the heat transfer coefficient (HTC) between the material and the quenching medium, has been added in the above expressions.

3. Formulation of criteria for fracture due to thermal shock

3.1. Longitudinal plies

Following the methodology developed for UD CMCs in [7], we postulate that cracking (in the form of PMCs) commences in the 0° plies when the total magnitude of the

applied thermal stresses in the matrix along the axial (x -) direction, $\sigma_{1,M}^{\text{th}}$, becomes equal to the matrix strength, σ_{mu} , i.e. when:

$$\sigma_{1,M}^{\text{th}} = \sigma_{mu} \quad (17)$$

In the case of cross-ply laminates, $\sigma_{1,M}^{\text{th}}$ comprises contributions from the applied thermal shock-induced stress in the axial direction, $\sigma_{1,M}^{\text{TS}}$, a residual thermal stress component at the ply level due to differences in CTE between the matrix and the fibre, $\sigma_{1,M}^{\text{RES}}$, as well as residual thermal stresses at the laminate level due to differences in CTE between 0° and 90° plies, $\sigma_{L,M}^{\text{RES}}$. The matrix fracture stress, σ_{mu} , can be derived from the classic ACK model [7, 13]. Thus, (17) can be written as:

$$\sigma_{1,M}^{\text{TS}} + \sigma_{1,M}^{\text{RES}} + \sigma_{L,M}^{\text{RES}} = \left(6\tau G_m E_m E_f V_f^2 / E_1 r V_m\right)^{1/3} \quad (18)$$

where r is the fibre radius and G_m the matrix fracture energy. The value of $\sigma_{1,M}^{\text{TS}}$ is found from multiplying (14) by E_m/E_1 . From (18) through (1), (3) and (14), we derive an expression for the value of the interfacial shear stress, τ , as a function of the applied temperature differential, ΔT , as:

$$\tau = \left(E_1 r V_m / 6G_m E_m E_f V_f^2\right) \left[\left(E_m A Q_{x,L} \Delta T / E_L\right) + \Theta_1 \Delta T_F + \left(E_m \Theta_L \Delta T_F / E_L\right) \right]^3 \quad (19)$$

By considering stresses perpendicular to the fibre-matrix interface (y -direction), i.e. the transverse component of the thermal shock-induced stress, σ_y^{TS} , the component of the residual thermal stresses at the ply level that acts at right angles to the interface, $\sigma_{2,M}^{\text{RES}}$, and the fibre roughness-induced compressive stress at the fibre-matrix interface, σ_2^{RA} , the effective value of the interfacial shear stress during thermal shock treatment can also be described (neglecting possible Poisson effects) by the following Coulomb-type expression:

$$\tau = -\mu \left[\sigma_{2,M}^{\text{RES}} + \sigma_y^{\text{TS}} + \sigma_2^{\text{RA}} \right] \quad (20)$$

where μ is the coefficient of friction between the fibre and the matrix. Through (4) and (16), and since the roughness-induced stress can be written as $-CA_r/r$ (where A_r is the roughness amplitude of the fibre surface and $C = E_m E_f / [E_f (1 + \nu_m) + E_m (1 - \nu_f)]$), (20) becomes:

$$\tau = -\mu \left[\left(\Theta_2 \Delta T_F\right) + \left(A Q_y \Delta T\right) + \left(-CA_r/r\right) \right] \quad (21)$$

The value of μ is obtained by applying (21) at room temperature (where $\sigma_y^{\text{TS}} = 0$) using experimentally-determined values of τ reported in the literature [7]. When both (19) and (21) are plotted against the applied quenching temperature differential in the same graph for a pre-determined value of the stress reduction factor,

they intersect at a particular ΔT , which is the critical temperature differential (ΔT_c) for the onset of multiple matrix cracking of the longitudinal ply.

3.2. Transverse plies

Following (17), we can postulate that cracking due to thermal shock in the 90° plies of cross-ply laminates commences when the applied thermal stresses, σ_T^{th} , become equal to the ply strength. However, as the 90° ply strength cannot be defined with any certainty using micromechanics considerations, we employ a fracture mechanics-based criterion and assume that cracking initiates when the applied thermal stress intensity factor, K_I^{th} , becomes equal to the fracture toughness of the transverse ply, K_{IC} . Considering the largest inherent central surface flaw of length $2c$ (and, obviously, ignoring the statistical distribution of flaw sizes on the ply surface), the criterion for fracture can be written as:

$$K_I^{\text{th}} = K_{IC} = \sigma_T^{\text{th}} \sqrt{\pi c} \quad (22)$$

In the transverse plies of cross-ply CMCs, HMCs (i.e. cracks that channelled along the x-direction) were observed. This means that in (22) the applied thermal stress, σ_T^{th} , is equal to the transverse component of the thermal shock-induced stress, σ_y^{TS} (there are no thermal residual stresses along the y-direction). In this way, the critical temperature differential for crack onset is given, through (16), by:

$$\Delta T_c = K_{IC} / A Q_y \sqrt{\pi c} \quad (23)$$

The fracture toughness of the transverse ply is given by:

$$K_{IC} = \sqrt{G_T E_2 / (1 - \nu_{23}^2)} \quad (24)$$

where G_T , is the fracture energy and ν_{23} can be assumed to be equal to ν_{21} .

However, since the value of the length of the initial surface flaw $2c$ can only be the result of an informed assumption, an alternative fracture mechanics-based criterion may be formulated by taking into consideration the analysis of Zhao *et al.* [14]. In this case, the applied thermal stress intensity factor can be written as a function of a critical dimension, t_c , which is defined as the minimum material dimension (usually the half-thickness) required for the applied thermal shock-induced stress to attain its maximum possible value (see below for detailed explanation). Formulation of this criterion (full derivation given in Appendix 1) leads to the following expression for the critical temperature differential:

$$\Delta T_c = K_{IC} / A' Q_y \sqrt{\pi t_c} \quad (25)$$

In (25), A' describes a form of the stress reduction factor derived through the work of Zhao *et al* [14] specifically for channelling cracks on the surface of thermally shocked solids.

3.3. The stress reduction factor

The values of the stress reduction factors (A and A') are crucial for successful application of the above criteria. They can be written analytically as (see Appendix 2):

$$A = [1.5 + (3.96k/th) - 0.5e^{-(33.5k/th)}]^{-1} \quad (26)$$

$$A' = (4.5 + 9.57k/th)^{-1} \quad (27)$$

In (26) and (27), th/k defines the Biot modulus β , a parameter that describes the heat transfer conditions, where k is the through-thickness thermal conductivity of the material, h the heat transfer coefficient and t a material dimension, usually the half-thickness. Both A and A' take their maximum possible values for specific heat transfer conditions (as characterised by h) when t is *at least* equal with the previously mentioned critical value, i.e. $t=t_c$. In case $t>t_c$, the stress reduction factors do not increase any further [1,2]. Thus, assuming that t_c is known, if the actual half-thickness of the shocked material is equal or larger than t_c we enter $t=t_c$ in (26) and (27), while if the actual half-thickness is smaller than t_c we employ that value and obtain the reduced values of A and A' . The value of the critical thickness, t_c , for particular shock conditions can be obtained by manipulating (26) and (27) using previous theoretical results (e.g. [7]) and suitable experimental results from the literature.

4. Application of fracture criteria to thermally-shocked cross-ply Nicalon®/CAS

4.1. Predictions of thermal shock resistance

The simple models developed in section 3 are applied now for making predictions of the thermal shock resistance of the range of cross-ply Nicalon®/CAS laminates investigated experimentally in [9] and [10], i.e. simple $[0/90]_s$, $[90/0]_s$ laminates ~0.72mm thick and multi-layer $[0/90]_{3s}$, $[90/0]_{3s}$, $[0_2/90_4]_s$ laminates of thickness ~2.2mm (relevant properties given in Tables 1a and 1b). As cracking due to thermal shock was found to initiate inside the central plies of each laminate, the criterion developed for multiple matrix cracking in 0° plies is applicable to $[90/0]_s$ and $[90/0]_{3s}$ lay-ups, while equations (23) and (25) are applicable to $[0/90]_s$, $[0/90]_{3s}$ and $[0_2/90_4]_s$ laminates.

Table 1a

Table 1b

For the multi-layer laminates, the stress reduction factor, A , is taken to be equal to $A=0.53$ [7]. Using this value together with the experimentally-determined value of the critical thickness in water-quenching of a similar material (i.e. one with comparable k and ΔT_c), we obtain through (26) the critical thickness of Nicalon®/CAS ($t_c \approx 0.8\text{mm}$) and the reduced value of A for the simple laminates ($A=0.43$), and through (27) the respective values of A' for multi-layer and simple laminates ($A'=0.18$, $A'=0.15$) (see Appendix 3). In addition, bearing in mind the work of Pryce and Smith [11][†], we assume that the initial flaw length entering (23) is of the order of the half-thickness of the central plies, i.e. $2c=0.183\text{mm}$ for the $[0/90]_{3s}$ and $[0/90]_s$, and $2c=0.733\text{mm}$ for the $[0_2/90_4]_s$ laminate. Finally, the transverse fracture energy, G_T , of Nicalon®/CAS entering (23) and (25) (through (24)) has been found experimentally to be approximately equal to the fracture energy of the matrix, G_m [15].

The plots of (19) and (21) for the central 0° plies of the $[90/0]_s$ and $[90/0]_{3s}$ laminates are shown in the graph of figure 3 and the deduced values of ΔT_c are presented in Table 2. Predictions through (23) and (25) for the 90° central plies of the $[0/90]_s$, $[0/90]_{3s}$ and $[0_2/90_4]_s$ laminates are also presented in Table 2.

Figure 3

Table 2

From the results, it can be seen that the accuracy of predictions for the central 0° plies of the $[90/0]_s$ and $[90/0]_{3s}$ laminates is excellent as the error in the predicted values is only 0.8-2.25%. Agreement with experimental data for $[0/90]_s$ and $[0/90]_{3s}$ laminates using (23) and for all laminates with central 90° plies using (25) is fair (error 11-20%). By contrast, the prediction for the $[0_2/90_4]_s$ laminate based on (23) displays a large discrepancy with the experimentally-determined value.

4.2. Discussion

The results presented in the previous paragraph provide further evidence for the validity of the approach adopted for predicting the thermal shock resistance in UD CMCs [7], i.e. for 0° plies. The method, that takes into consideration the anisotropic stress field and the effect of the shock on the effective value of the interfacial shear stress, was applied successfully to the central 0° plies of two different lay-ups and accurate estimates of their resistance to thermal shock were obtained.

The success in the prediction for the $[90/0]_s$ laminate, which captures the difference in ΔT_c with the $[90/0]_{3s}$, and the clear differentiation achieved between the predicted values for $[0/90]_s$ and $[0/90]_{3s}$ laminates indicate that the simple method utilising equations (26) and (27) to account for reduced material thickness can

[†] Pryce and Smith [11] argue that $[0/90]_{3s}$ and $[0_2/90_4]_s$ cross-ply Nicalon®/CAS laminates exhibit what is termed 'unconstrained' cracking under monotonic tensile loading, i.e. the pre-existing critical flaw is smaller than the thickness of the central 90° plies. They also came to the conclusion that the initial flaw in the eight central plies of the $[0_2/90_4]_s$ laminate can be considered to be longer than the one in the central double transverse ply of the $[0/90]_{3s}$.

adequately capture the so-called ‘thickness effect’ in the observed thermal shock resistance of ceramic materials. However, it must be noted that the success of the method depends on the validity of the expression describing the stress reduction factor and the availability of suitable experimental data, which will allow the determination of the critical dimension of the material at specific quenching temperature differentials.

Concentrating on the laminates with 90° central plies, the expression based on Zhao *et al.* [14], utilising the critical dimension of the material, yielded reasonable but conservative results. The observed conservatism may be a product of the value of the fracture toughness of the transverse ply, K_{IC} , entered in the calculations. HMCs originate on the surface at ΔT_c and advance along the ply length without extending significantly into the bulk of the material, while being continuously deflected around successive fibre ends [10]. It can be argued that this situation resembles crack deflection in ceramics containing spherical reinforcements [16, 17] and that there may be an increased, apparent value of fracture toughness for the particular cracking mode. Performing a parametric study (using $K'_{IC} = K_{IC} \sec(\theta/2)$), it can be shown that if a small angle of deflection (as observed experimentally) of $\theta=45^\circ$ is assumed, in which case the effective fracture toughness of the 90° ply increases by a factor of 1.17, satisfactory predictions can be obtained. More specifically, (25) gives $\Delta T_c=363^\circ\text{C}$ for the $[0/90]_{3s}$ laminate, $\Delta T_c=436^\circ\text{C}$ for the thinner $[0/90]_s$ lay-up, and $\Delta T_c=399^\circ\text{C}$ for the $[0_2/90_4]_s$ CMC, i.e. the error in the predictions is reduced to 0.25-3%.

Finally, two points need to be made regarding the predictions of the thermal shock resistance of the $[0_2/90_4]_s$ laminate. First, it was successfully predicted through (25) that this laminate exhibits higher ΔT_c than the $[0/90]_{3s}$ CMC. This can be attributed to the lower value for the transverse ply modulus, E_2 , employed in the calculations for the $[0_2/90_4]_s$ lay-up, which was deduced from experimental results (see Table 1). If the Voigt estimate for E_2 had been utilised, the respective resistances to thermal shock for these two multi-layer cross-ply CMCs with 90° central plies would have been almost identical.

Second, the very big discrepancy (~57% error) that can be observed in the prediction of the thermal shock resistance of the $[0_2/90_4]_s$ laminate through (23) reveals that the assumption regarding the initial flaw size for this material was erroneous. However, this should have been expected since cracking initiates at the central portion of each laminate, which, as can be concluded by the behaviour of the other lay-ups, is significantly thinner than the eight central 90° plies of the $[0_2/90_4]_s$. In addition, contrary to what was observed under tensile testing (where the $[0_2/90_4]_s$ CMC displayed a lower matrix cracking stress than the $[0/90]_{3s}$) [11], the $[0_2/90_4]_s$ has a higher ΔT_c than the $[0/90]_{3s}$ laminate. This means that a significantly smaller flaw size determines the strength of the transverse ply under thermal shock than the one selected. Indeed, if we employ the same flaw size with that selected for the other laminates with 90° central plies, the error in the calculation can be reduced to 15% ($\Delta T_c=342^\circ\text{C}$) or zero ($\Delta T_c=400^\circ\text{C}$ for $K=1.17K_{IC}$).

5. Crack morphology

5.1. Introduction

1
2
3 The observation that thermal shock cracking always originates at the central area of
4 each exposed face and not at a corner was reported in [10] for cross-ply laminates. On
5 application of larger shocks ($\Delta T > \Delta T_c$) damage appeared within the outer plies but the
6 crack density displayed a gradient, with the highest value at the central area and
7 reducing gradually towards the outer plies. The same phenomenon has also been
8 reported for UD, angle-ply and woven Nicalon®/CAS laminates [4,5] and has been
9 observed on water-quenched Cerasep® 410 SiC/SiC laminates [18]. It implies that a
10 gradient exists in the value of the shock-induced stresses across the laminate face, with
11 maximum values at the central area reducing towards the outer plies. A possible
12 explanation, based on thermal shock theory, for this phenomenon is provided in this
13 section.
14
15
16
17
18
19
20
21

22 5.2. Analysis

23 We consider that the surfaces of a CMC in figure 4 (for clarity, the alternating plies are
24 not shown), held at a high temperature T_s , come into contact with a medium of much
25 lower temperature T_o . At this point, a temperature gradient is established between *each*
26 surface ($1, 2A, 2B, 3A, 3C$) and the inner part of the material.
27
28
29

30 Figure 4

31 According to thermal shock theory, this results in the appearance of a distribution of
32 compressive stresses inside the body that are balanced by a distribution of tensile
33 stresses close to each surface. The maximum biaxial tensile stresses are induced *at* each
34 surface. As referred to previously, for β to attain its maximum value (and thus A and
35 the shock-induced stresses) for prescribed HTC, their minimum dimension (usually
36 their half-thickness, t) must be *at least* equal with a critical value, i.e. $t = t_c$. If $t < t_c$,
37 the Biot modulus β does not take its maximum possible value, and thus A and the induced
38 stress do not attain their maximum values. For $t > t_c$, the value of β becomes independent
39 of material dimensions (i.e. does not increase any further). The three conditions are
40 illustrated in the schematics of figure 5.
41
42
43

44 Figure 5

45
46 Returning to figure 4 and concentrating on surface 1 , we observe that the
47 critical dimensions of the top and bottom surfaces (t_c^{3A} and t_c^{3B}) do not overlap, which
48 corresponds to the case where $t > t_c$. The same is true for the critical dimensions of the
49 opposing side faces (t_c^{2A} and t_c^{2B}). However, we also notice that with regards to surface
50 1 , except for the volume enclosed by the red lines, the respective critical dimensions of
51 the adjoining surfaces *do* overlap. We can postulate that the situation at these material
52 sections corresponds to the situation where $t < t_c$. This means that here the thermal
53 shock-induced stress does not attain its maximum possible value as the value of the
54 Biot modulus is reduced. The value of t can be thought of as varying on surface 1
55 from zero at each corner to $t = t_c$ at each red line. In contrast, the volume bound by the
56 red lines (for which $t \geq t_c$ everywhere) will experience the maximum possible severity of the
57 applied thermal shock.
58
59
60

It must be noted that if t_c^{3A} was equal to t_c^{3B} , the volume of maximum thermal
shock-induced stress (red volume) would reduce to a parallelogram. In addition, even if

1
2
3 t_c^{3A} and t_c^{3B} overlapped and the maximum possible stress value could not be attained, a
4 gradient of stress would exist across the surface being higher at the central portion and
5 reducing to zero towards the top and bottom corners.
6
7
8
9

10 **5.3. Discussion**

11
12 The above analysis provides the background for a satisfactory explanation of the
13 cracking phenomena on thermally shocked Nicalon®/CAS laminates. As the central
14 area of each surface experiences the maximum applied stress due to thermal shock, it is
15 the region where initial damage appears. With increasing shock severity, damage will
16 appear at the other areas of the surface but the maximum stress, and thus crack density,
17 will always be at the central area. In addition, as the applied shock-induced stress at
18 each ΔT decreases from the central area towards the edges, a corresponding gradient of
19 crack density across the surface will become evident.
20
21

22 In the case of the simple cross-ply laminates ($[0/90]_s$ and $[90/0]_s$) of thickness
23 $\sim 0.72\text{mm}$, t_c^{3A} and t_c^{3B} do overlap (figure 5c, since $t_c^{3A}=t_c^{3B}=0.8\text{mm}$ is much higher than
24 their half-thickness of 0.36mm) and, thus, the shock-induced stresses do not attain their
25 maximum possible values. The result is that these laminates display a higher resistance
26 to thermal shock than their thicker, multi-layer counterparts investigated in [9] and
27 [10], which have a thickness of $\sim 2.2\text{mm}$. In these laminates t_c^{3A} and t_c^{3B} do not overlap
28 (figure 5b, since $t_c^{3A}=t_c^{3B}=0.8\text{mm}$ is lower than their half-thickness of 1.1mm), and,
29 thus, there is a central area $\sim 0.6\text{mm}$ wide ($2.2-2\times 0.8$) that receives the maximum
30 possible thermal shock severity. The width of this area corresponds to the equivalent of
31 approximately three plies ($0.6/0.183$), i.e. the two central plies of each laminate and a
32 portion of each ply adjacent to them, and it is where damage first appears and remains
33 higher on application of higher shocks. The same reasoning can be extended to the case
34 of UD, angle-ply and woven Nicalon®/CAS laminates of comparable thickness to
35 explain crack patterns during thermal shock treatment [4,5].
36
37

38 In addition, as the stress reduction factor can be thought of as varying across the
39 shocked surface, we can proceed to predictions for the thermal shock resistance of the
40 outer plies if we prescribe a function to describe the variance of the stress reduction
41 factor across the surface. The most obvious assumption that can be made is that this
42 dependence can be described by a function similar to that describing the dependence of
43 A and A' to the depth dimension, i.e. (26) and (27). Such an approach, though
44 simplistic because different conditions (A and h) are prevalent at higher shocks, can
45 yield reasonable results, as can be seen in Appendix 4.
46
47

48 Finally, the analysis of this section can also provide an explanation for the
49 behaviour of cracks in the 90° plies of cross-ply laminates. Computations using the
50 formulas developed in the stress analysis part of this paper (section 2) reveal that a very
51 small difference between the total axial and transverse stresses (shock-induced and
52 residual) applied to the 90° plies exists at all ΔT s. The prevalence of cracks that
53 advance horizontally, i.e. along the x -direction (HMCs), is probably the result of the
54 nature of the applied stress field combined with local stress variations; the cracks
55 originate inside each 90° ply and simply follow the path perpendicular to which the
56 maximum, continuous and constant thermally-induced stress is applied, i.e. the x -
57 direction. In addition, local stress variations guide the crack always through areas of
58 high fibre volume fraction and away from the interfacial zones with adjacent 0° plies.
59 Further, it may be that within the central plies of the laminate there are a greater
60

number of larger defects parallel to the x-direction than parallel to the y-direction (figure 2). Such defects might arise from processing and potentially could be larger in the x-direction than in the y-direction because there is no constraint from neighbouring layers associated with the x-direction. Such effects would promote the formation of HMCs.

6. Concluding Remarks

Analytical predictions regarding the onset of matrix cracking due to thermal shock in a range of cross-ply Nicalon®/CAS laminates (simple $[0/90]_s$ and $[90/0]_s$, multi-layer $[0/90]_{3s}$, $[90/0]_{3s}$ and $[0_2/90_4]_s$) were presented in this study. The predictions were made by combining a comprehensive steady-state stress analysis of the materials under thermal shock with suitable fracture criteria and a method utilizing the stress reduction factor to account for thickness effects on thermal shock behaviour.

For the laminates with 0° central plies ($[90/0]_s$ and $[90/0]_{3s}$) the fracture criterion was based on the approach developed by the same authors for predicting the thermal shock resistance of UD Nicalon®/glass ceramic-matrix composites, including Nicalon®/CAS, and yielded predictions of excellent accuracy for both simple and multi-layer CMCs. Two fracture criteria based on fracture mechanics considerations were employed for the laminates with 90° central plies ($[0/90]_s$, $[0/90]_{3s}$ and $[0_2/90_4]_s$) and produced satisfactory results as the main trends in the behaviour of these laminates under thermal shock were modelled successfully. Some discrepancies identified in the resulting predictions were attributed to the values of individual parameters entering the model.

In addition, a theoretical argument emanating from thermal shock theory was proposed to explain some characteristics of the cracking pattern on fibre-reinforced CMCs under conditions of thermal shock. The argument was based on the concept of the existence of a critical material-specific dimension at each ΔT for the applied shock-induced stress to attain its maximum possible value, normally used to explain the so-called 'thickness effect' on thermal shock resistance. Subsequent analysis provided an insight into why damage at fracture onset (ΔT_c) always appears at the central plies of fibre-reinforced CMCs and why a crack density gradient exists at higher temperature differentials.

Appendix 1

The analysis of Zhao *et al.* [14] considers the variation of the full thermo-elastic stress field across the through-thickness direction and utilises fracture mechanics by assuming a pre-existing flaw in the depth direction.

Figure 6

In figure 6, a component with thickness $2H$ is subjected to thermal shock at the top and bottom faces. The authors assume that there is a pre-existing crack of length H and,

based on this, derive expressions for the applied stress intensity factor due to thermal shock taking into account the varying nature of the applied stress across the thickness. According to thermal shock theory, the half-thickness H should be equal to or greater than a critical dimension, t_c , such that the stress at the top and bottom faces can reach its maximum value, i.e. $H \geq t_c$. If H is made equal to the critical dimension, t_c , the equation derived by Zhao *et al.* for crack channelling (i.e. growth in the x-direction) has the form:

$$K_I^{TS} = A' Q_3 \Delta T \sqrt{\pi c} \quad (28)$$

where $A' = A''/\sqrt{\pi}$ and $A'' = (2.54 + 5.4/\beta)^{-1}$. Thus:

$$A' = (4.5 + 9.57/\beta)^{-1} \quad (29)$$

Appendix 2

The stress reduction factor, A , is usually given by a formula of the form [1,2]:

$$A = [a + (b/\beta) - ce^{(d/\beta)}]^{-1} \quad (30)$$

This formula describes a function fitted to the variation of the transient thermo-elastic stress field between the surface and the inner part of the material, derived by taking into account the temperature gradient due to the shock as well as the shape of the material (e.g. [19]). The parameters a , b , c , d depend on the shape of the component; for an infinite plate $a=1.5$, $b=3.25$, $c=0.5$ and $d=-16$ whereas for an infinite rod $a=1.5$, $b=4.67$, $c=0.5$, $d=-51$ [20]. When dealing with rectangular specimens (as it is the case here), it is usual practise to adopt values between these two extremes (e.g. [21]); in this case we simply use their averages, i.e. $a=1.5$, $b=3.96$, $c=0.5$, $d=-33.5$. Through the Biot modulus, β , (30) becomes:

$$A = [1.5 + (3.96k/th) - 0.5e^{-(33.5k/th)}]^{-1} \quad (31)$$

In this formula, thermal conductivity k is given in the case of cross-ply CMCs by rule of mixtures estimates using for the 0° ply $k = k_f k_m / (k_f V_m + k_m V_f)$ and for the 90° ply $k = k_m V_m + k_f V_f$.

The stress reduction factor, A' , is given, through the Biot modulus, by [14]:

$$A' = (4.5 + 9.57k/th)^{-1} \quad (32)$$

Appendix 3

For UD Nicalon®/CAS, which is of comparable thickness with the multi-layer cross-ply Nicalon®/CAS laminates, $A=0.53$ was obtained in [7]. Using this value and the

1
2
3 data available for a water-quenched glass ceramic of comparable properties and thermal
4 shock resistance ($\alpha=4.5 \times 10^{-6} \text{ K}^{-1}$, $k=3.5 \text{ Wm}^{-1}\text{K}^{-1}$, $\Delta T_c \cong 430^\circ\text{C}$, $t_c=1.15\text{mm}$) [22], we
5 deduce through (26) a value of $h \approx 30 \text{ kWm}^{-2}\text{K}^{-1}$. Re-applying (26) with this value of h ,
6 A equal to 0.53 and the thermal conductivity of the composite, we obtain $t_c \cong 0.8\text{mm}$ for
7 cross-ply Nicalon®/CAS. In other words, we assume that the heat transfer conditions
8 (as characterised by A and h) during water-quenching of two materials with
9 comparable properties and thermal shock resistance are the same.
10
11

12
13 The reduced stress reduction factor for the simple cross-ply laminates ($[0/90]_s$, $[90/0]_s$),
14 which have a half-thickness of $\sim 0.36\text{mm}$, is found to be $A \cong 0.43$ by entering in (26) the
15 deduced value of h ($h \approx 30 \text{ kWm}^{-2}\text{K}^{-1}$) and the half-thickness of the materials. Finally,
16 the parameter A' is calculated to be 0.18 for the thicker, multi-layer CMCs (which are
17 $\sim 2.2\text{mm}$ thick) and 0.15 for the simple laminates, by entering in (27) $h \approx 30 \text{ kWm}^{-2}\text{K}^{-1}$
18 together with $t_c=0.8\text{mm}$ (for the thicker materials, since $2t_c < 2.2\text{mm}$) and $t=0.36\text{mm}$ (for
19 the simple laminates).
20
21
22
23

24 Appendix 4

25
26 For each cross-ply Nicalon®/CAS laminate, the value of t in (26) and (27) on the
27 surface in question can be thought of as varying from $t=0$ at each corner to $t=t_{lam}/2$ (for
28 simple laminates) or $t=t_c$ (for multi-layer laminates) at the centre. To obtain a prediction
29 for each ply, we must enter for t the coordinate of each ply along the y-direction. This
30 is shown in figure 7 for $[0/90]_{3s}$ and $[90/0]_{3s}$ laminates together with the derived values
31 of the stress reduction factor. It must be noted that the schematic of figure 7
32 corresponds to the $[0/90]_{3s}$ lay-up; for the $[90/0]_{3s}$ laminate we simply alter the ply
33 sequence. Predictions for each longitudinal ply using (19) and (21), and for each
34 transverse ply using (25) (with $K=1.17K_{IC}$) are shown in Table 3.
35
36
37

38 Figure 7

39 Table 3

40 Acknowledgements

41
42 CK wishes to acknowledge financial support from the Engineering and Physical
43 Sciences Research Council (EPSRC) of the UK and the 'Alexander S. Onassis' Public
44 Benefit Foundation. PAS and JAY would like to acknowledge the encouragement that
45 they received from Professor Kelly in the late 1980s to pursue research on ceramic
46 matrix composites. Twenty years on, they can both recall memorable discussions
47 with Professor Kelly during the course of lengthy car journeys from Guildford to
48 Derby.
49
50
51
52
53
54
55
56
57
58
59
60

References

- 1
2
3
4
5 [1] H. Wang and R.N. Singh, *Int. Mater. Rev.* 39 (1994) p.228
6 [2] C. Kastritseas, P.A. Smith and J.A. Yeomans, *Thermal shock of ceramic matrix*
7 *composites*, in *Ceramic Matrix Composites: Microstructure, Properties and*
8 *Applications*, J. Low, ed., Woodhead Publishing Ltd., 2006, p.400
9 [3] H. Wang, R.N. Singh and R.A. Lowden, *J. Am. Ceram. Soc.* 79 (1996) p.1783
10 [4] M.J. Blissett, P.A. Smith and J.A. Yeomans, *J. Mater. Sci.* 32 (1997) p.317
11 [5] C. Kastritseas, P.A. Smith and J.A. Yeomans, *J. Mater. Sci.* 43 (2008) p.4112
12 [6] H. Mei, L. Cheng, *Mater. Sci. Eng. A* 486 (2008) p.235
13 [7] C. Kastritseas, P.A. Smith and J.A. Yeomans, *Compos. Sci. Technol.* 65 (2005)
14 p.1880
15 [8] A.R. Boccaccini, *Scripta Mater.* 38 (1998) p.1211
16 [9] M.J. Blissett, P.A. Smith and J.A. Yeomans, *J. Mater. Sci.* 33 (1998) p.4181
17 [10] C. Kastritseas, P.A. Smith and J.A. Yeomans, *J. Mater. Sci.* 41 (2006) p.951
18 [11] A.W. Pryce and P.A. Smith, *J. Mater. Sci.* 27 (1992), p.2695
19 [12] C. Kastritseas, *Fracture of Fibre-Reinforced Ceramic-Matrix Composites*
20 *Under Conditions of Thermal Shock*, Ph.D. Thesis, University of Surrey, 2005
21 [13] J. Aveston, G.A. Cooper and A. Kelly, *Single and multiple fracture*, in *The*
22 *Properties of Fibre Composites*, IPC Science & Technology Press, Guildford,
23 UK, 1971, p.15
24 [14] L.G. Zhao, T.J. Lu and N.A. Fleck, *J. Mech. Phys. Solids* 47 (2000) p.867
25 [15] R. Kahraman, J.F. Mandell and M.C. Deibert, *J. Am. Ceram. Soc.* 80 (1997)
26 p.1812
27 [16] K.T. Faber and A.G. Evans, *Acta Metall.* 31 (1983) p.565
28 [17] S.M. Wiederhorn and E.R. Fuller Jr., *Structural Behaviour of Ceramics*, in
29 *Comprehensive Structural Integrity*, I. Milne, R.O. Ritchie and B. Karihaloo,
30 eds., Elsevier Science Ltd., 2003, Vol. 2, p.429
31 [18] C. Kastritseas, P.A. Smith and J.A. Yeomans, unpublished work
32 [19] T.J. Lu and N.A. Fleck, *Acta Mater.* 46 (1998) p.4755
33 [20] S.S. Manson, *Thermal Stress and Low-Cycle Fatigue*, McGraw-Hill Book
34 Company, New York, 1966
35 [21] S. Maensiri and S.G. Roberts, *J. Am. Ceram. Soc.* 85 (2002) p.1971
36 [22] P.F. Becher and W.H. Warwick, *Factors influencing the thermal shock*
37 *behaviour of ceramics*, in *Thermal Shock and Thermal Fatigue Behaviour of*
38 *Advanced Ceramics*, G.A. Schneider and G. Petzow, eds., Kluwer Academic
39 Publishers, Dordrecht, The Netherlands, 1993, p.37
40
41
42
43
44
45
46
47
48
49
50
51
52
53
54
55
56
57
58
59
60

Table 1a. The properties of the Nicalon® fibre and the calcium aluminosilicate (CAS) matrix. From [7], [11] and [13].

Material	E (GPa)	α (10^{-6}K^{-1})	ν	Γ (J m^{-2})	r (μm)	k ($\text{Wm}^{-1}\text{K}^{-1}$)	A_r (nm)
Nicalon®	190	3.3	0.2	-	8	2.97	30
CAS	90	4.6	0.25	25	-	1.8	-

Table 1b. The properties of a unidirectional ply of Nicalon®/CAS taken from [7] and [11]. It should be noted that the values of E_2 were investigated extensively in [11]. The laminated plate theory value of 110 GPa was shown experimentally to be valid for the $[0/90]_s$ and $[0/90]_{3s}$ laminates but a reduced value of 90 GPa was found to be appropriate for the $[0_2/90_4]_s$ laminate.

Property	UD Nicalon®/CAS
V_f	0.34
E_1 (GPa)	124
E_2 (GPa)	90-110
α_1 ($10^{-6}K^{-1}$)	3.92
α_2 ($10^{-6}K^{-1}$)	4.26
ν_{12}	0.233
ν_{21}	0.212

Table 2. Predictions of the thermal shock resistance (water-quench) for the range of cross-ply Nicalon®/CAS CMCs investigated in [9] and [10]. The critical temperature differentials for the $[90/0]_s$ and $[90/0]_{3s}$ laminates (0° central plies) are deduced from figure 3. Predictions for the $[0/90]_s$, $[0/90]_{3s}$ and $[0_2/90_4]_s$ laminates (90° central plies) were obtained using (23) and (25). The % error in the predicted values compared with the experimentally-determined ones is also shown.

Laminate		$[90/0]_{3s}$	$[90/0]_s$	$[0/90]_{3s}$	$[0/90]_s$	$[0_2/90_4]_s$
ΔT_c ($^\circ\text{C}$)	Experimental	400	500	350	450	400
	Predicted					
	(19) & (21)	391	496	N/A	N/A	N/A
	(23)	N/A	N/A	312	359	171
	(25)	N/A	N/A	310	372	341
% Error		2.25	0.8	11	17-20	15-57

Table 3. Predictions of the thermal shock resistance (water-quench) for all plies of $[0/90]_{3s}$ and $[90/0]_{3s}$ Nicalon®/CAS laminates. Experimentally-determined values of the thermal shock resistance of each ply are shown in the parentheses.

Ply / Laminate	$[90/0]_{3s}$	$[0/90]_{3s}$
L1	496 (400-500)	>650 (500-600)
T1	543 (500-600)	434 (500-600)
L2	405 (400-500)	430 (400-500)
T2	383 (400-500)	372 (400-500)
L3	391 (400)	400 (400)
T3	362 (400)	363 (350)

1
2
3
4
5
6
7
8
9
10
11
12
13
14
15
16
17
18
19
20
21
22
23
24
25
26
27
28
29
30
31
32
33
34
35
36
37
38
39
40
41
42
43
44
45
46
47
48
49
50
51
52
53
54
55
56
57
58
59
60

Figure 1. A reflected light microscopy image of the surface of a thermally shocked (water quench) $[90/0]_{3s}$ Nicalon®/CAS laminate (after [12]). The formation of multiple PMCs is evident in the central 0° plies and a single HMC can be seen advancing along the length of one of the adjacent 90° plies.

Figure 2. A cross-ply composite subjected to thermal shock. Thermal shock-induced stresses as well as residual thermal stresses at the ply and laminate levels are also shown. The subscript 'L' denotes 0° ply whereas the subscript 'T' denotes 90° ply.

Figure 3. Predictions of the thermal shock resistance (water-quench) of $[90/0]_s$ and $[90/0]_{3s}$ Nicalon®/CAS laminates. Since these laminates contain 0° central plies, their resistance to thermal shock is dictated by the behaviour of these plies and its prediction is based on (19) - dashed lines, and (21) - continuous lines. The critical temperature differential (ΔT_c) is the ΔT at which the lines representing the two equations for each laminate intersect.

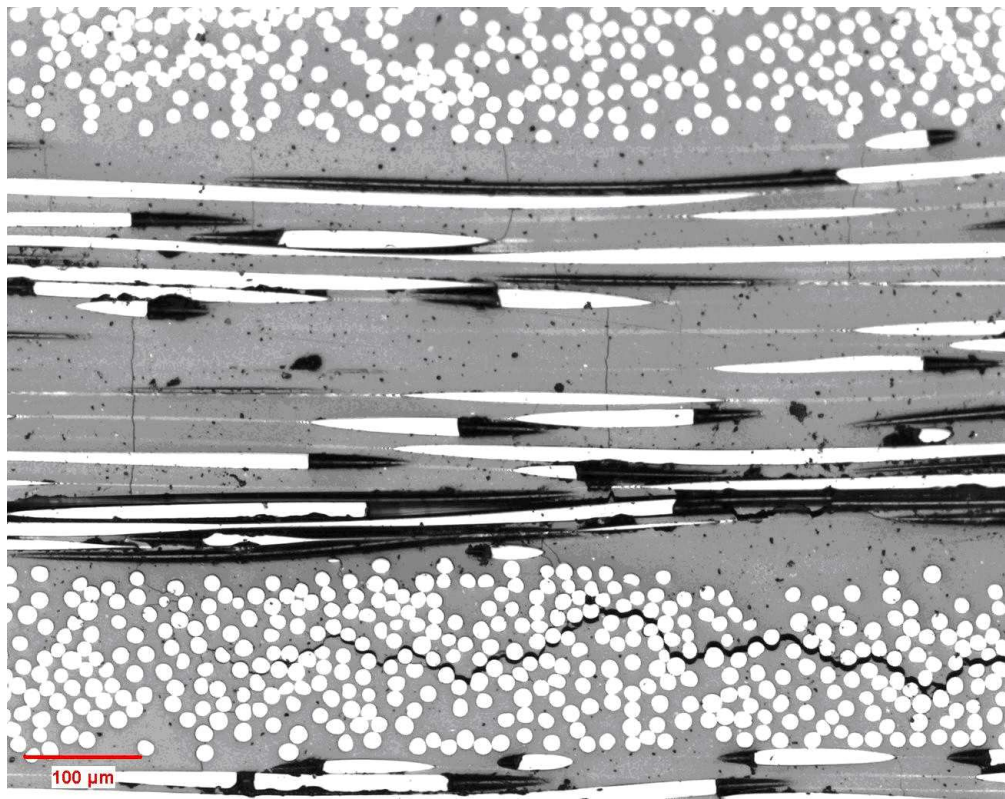
Figure 4. Schematic of the parallel face of a cross-ply CMC, where the critical dimensions of the adjoining faces have been superimposed. The volume in red corresponds to the space where thermal shock-induced stresses take their maximum value.

Figure 5. Schematics of a plate (thickness= $2t$) held at temperature T_s whose top and bottom faces are subjected to a lower temperature T_o (inducing a thermal shock $\Delta T=T_s-T_o$) for which (a) $t=t_c$, (b) $t>t_c$, and (c) $t<t_c$.

Figure 6. Schematic of a plate of thickness $2H$ whose top and bottom faces are subjected to thermal shock (after Zhao *et al.* [14])

Figure 7. Calculation of the stress reduction factors across the surface of a thermally-shocked (water quench) $[0/90]_{3s}$ Nicalon®/CAS laminate through (26) and (27). Due to symmetry, only half of the laminate is sketched. 'L' denotes 0° ply and 'T' 90° ply. For a $[90/0]_{3s}$ laminate the sequence is reversed. All dimensions in millimetres. Note that for $t>0.8\text{mm}$, $A=0.53$ and $A'=0.18$.

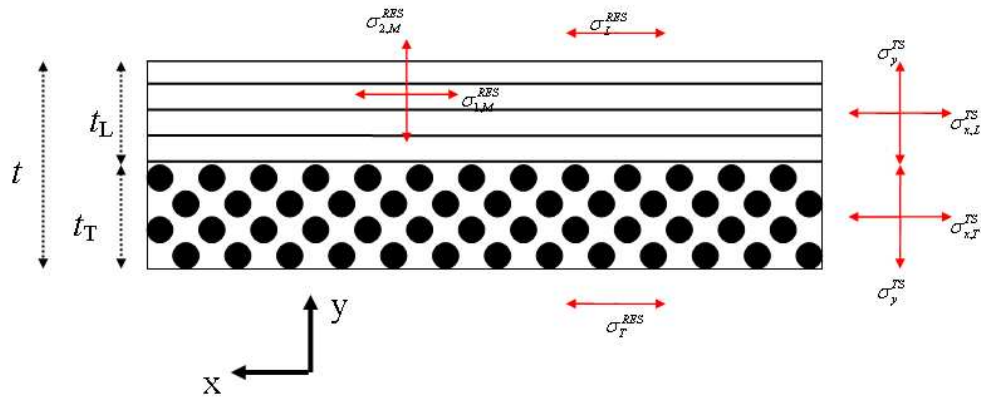
1
2
3
4
5
6
7
8
9
10
11
12
13
14
15
16
17
18
19
20
21
22
23
24
25
26
27
28
29
30
31
32
33
34
35
36
37
38
39
40
41
42
43
44
45
46
47
48
49
50
51
52
53
54
55
56
57
58
59
60



343x272mm (96 x 96 DPI)

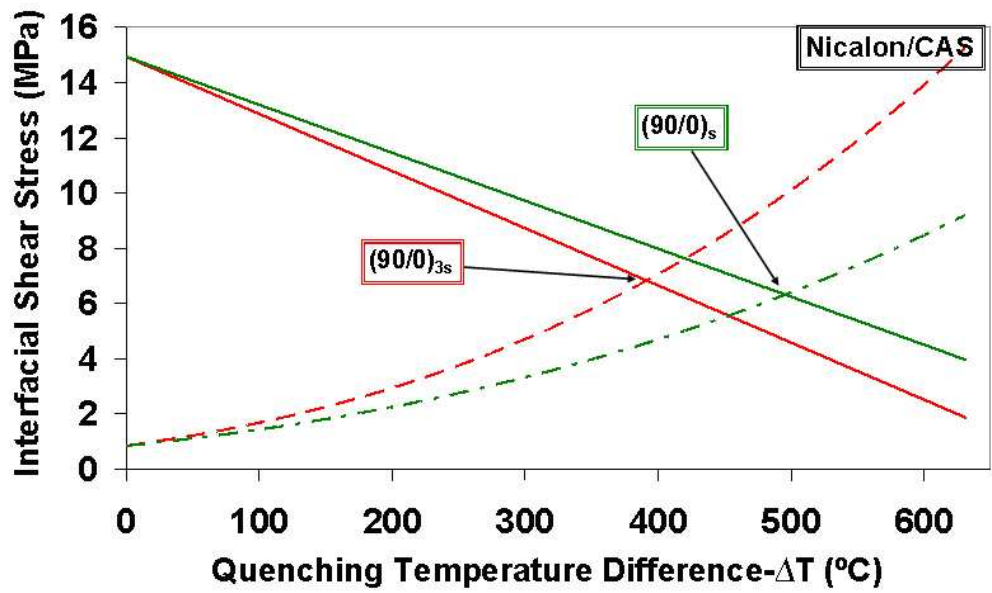
ew Only

1
2
3
4
5
6
7
8
9
10
11
12
13
14
15
16
17
18
19
20
21
22
23
24
25
26
27
28
29
30
31
32
33
34
35
36
37
38
39
40
41
42
43
44
45
46
47
48
49
50
51
52
53
54
55
56
57
58
59
60



210x89mm (96 x 96 DPI)

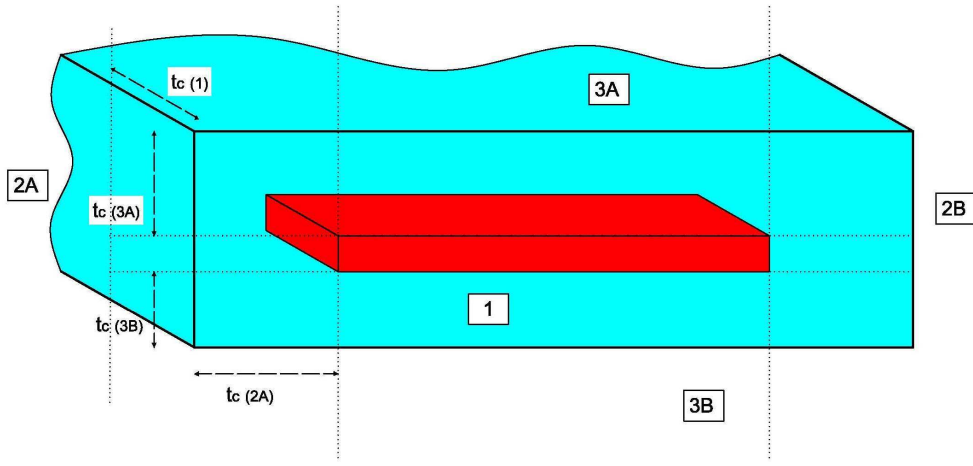
1
2
3
4
5
6
7
8
9
10
11
12
13
14
15
16
17
18
19
20
21
22
23
24
25
26
27
28
29
30
31
32
33
34
35
36
37
38
39
40
41
42
43
44
45
46
47
48
49
50
51
52
53
54
55
56
57
58
59
60



208x127mm (96 x 96 DPI)

Review Only

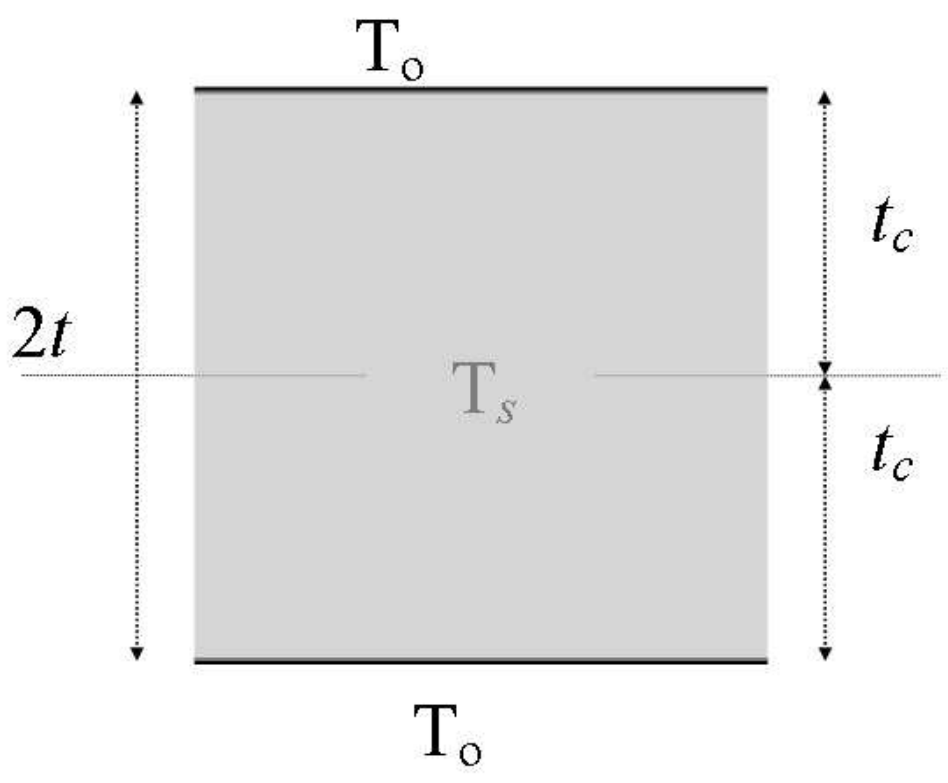
1
2
3
4
5
6
7
8
9
10
11
12
13
14
15
16
17
18
19
20
21
22
23
24
25
26
27
28
29
30
31
32
33
34
35
36
37
38
39
40
41
42
43
44
45
46
47
48
49
50
51
52
53
54
55
56
57
58
59
60



275x129mm (200 x 200 DPI)

er Review Only

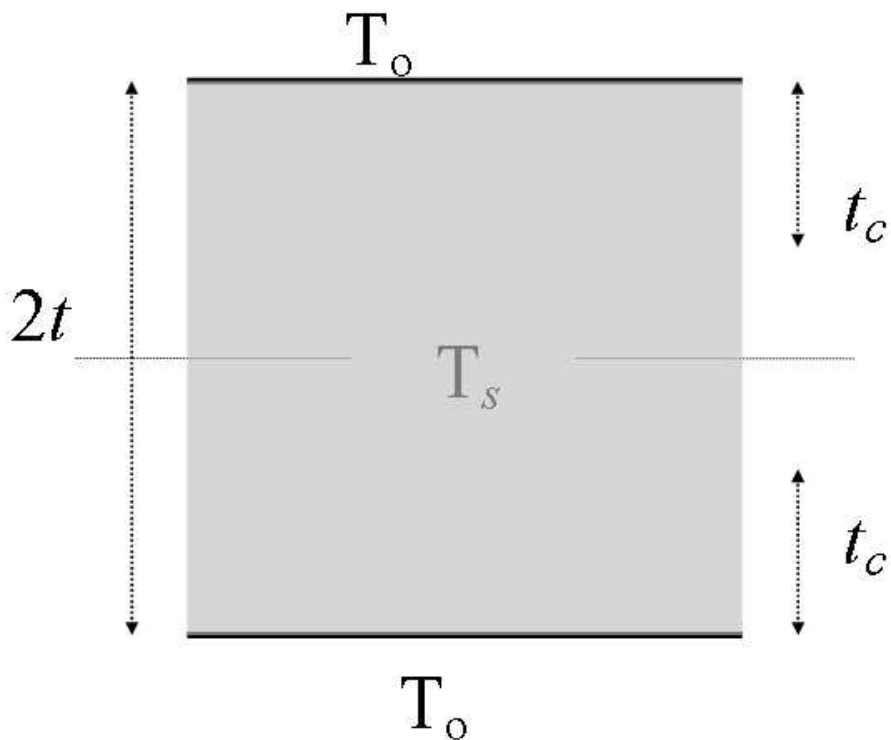
1
2
3
4
5
6
7
8
9
10
11
12
13
14
15
16
17
18
19
20
21
22
23
24
25
26
27
28
29
30
31
32
33
34
35
36
37
38
39
40
41
42
43
44
45
46
47
48
49
50
51
52
53
54
55
56
57
58
59
60



151x129mm (96 x 96 DPI)

Manuscript Only

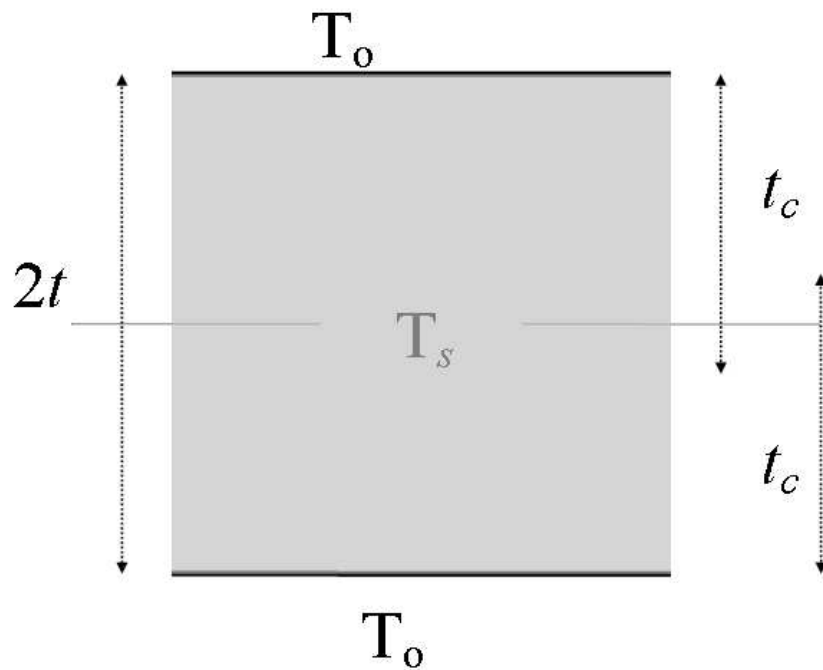
1
2
3
4
5
6
7
8
9
10
11
12
13
14
15
16
17
18
19
20
21
22
23
24
25
26
27
28
29
30
31
32
33
34
35
36
37
38
39
40
41
42
43
44
45
46
47
48
49
50
51
52
53
54
55
56
57
58
59
60



159x132mm (96 x 96 DPI)

View Only

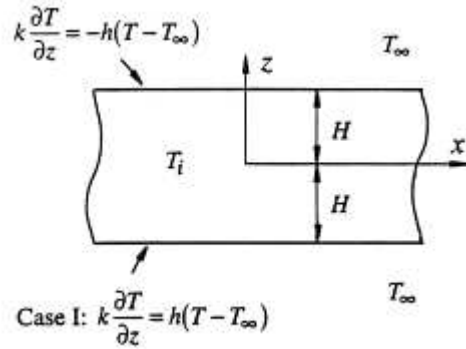
1
2
3
4
5
6
7
8
9
10
11
12
13
14
15
16
17
18
19
20
21
22
23
24
25
26
27
28
29
30
31
32
33
34
35
36
37
38
39
40
41
42
43
44
45
46
47
48
49
50
51
52
53
54
55
56
57
58
59
60



184x138mm (96 x 96 DPI)

new Only

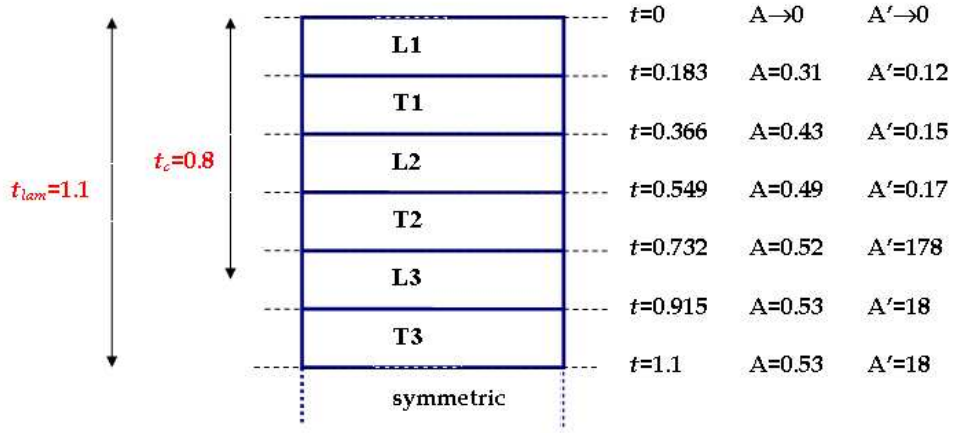
1
2
3
4
5
6
7
8
9
10
11
12
13
14
15
16
17
18
19
20
21
22
23
24
25
26
27
28
29
30
31
32
33
34
35
36
37
38
39
40
41
42
43
44
45
46
47
48
49
50
51
52
53
54
55
56
57
58
59
60



66x50mm (96 x 96 DPI)

Peer Review Only

1
2
3
4
5
6
7
8
9
10
11
12
13
14
15
16
17
18
19
20
21
22
23
24
25
26
27
28
29
30
31
32
33
34
35
36
37
38
39
40
41
42
43
44
45
46
47
48
49
50
51
52
53
54
55
56
57
58
59
60



192x94mm (96 x 96 DPI)

Review Only